TECHNIQUES AND RESOURCES

Chimeric 3D-gastruloids – a versatile tool for studies of mammalian peri-gastrulation development

Alexandra E. Wehmeyer[1], Katrin M. Schüle[1], Alexandra Conrad[1], Chiara M. Schröder[1,2,3,4], Simone Probst[1], and Sebastian J. Arnold[1,4]

[1]Institute of Experimental and Clinical Pharmacology and Toxicology, Faculty of Medicine, University of Freiburg, Albertstrasse 25, D-79104 Freiburg, Germany

[2]Spemann Graduate School of Biology and Medicine (SGBM), University of Freiburg, Albertstrasse 19a, D-79104 Freiburg, Germany

[3]Faculty of Biology, University of Freiburg, Schänzlestrasse 1, D-79104 Freiburg, Germany

[4]Signaling Research Centers BIOSS and CIBSS, University of Freiburg, Schänzlestrasse18, D-79104 Freiburg, Germany

Correspondence should be addressed to sebastian.arnold@pharmakol.uni-freiburg.de

ORCID Alexandra E. Wehmeyer 0000-0002-9981-8042
ORCID Katrin M. Schüle 0000-0001-6642-0030
ORCID Alexandra Conrad 0000-0001-7766-5033
ORCID Chiara M. Schröder 0000-0001-5345-3415
ORCID Simone Probst 0000-0002-0220-5400
ORCID Sebastian J. Arnold 0000-0002-2688-9210

Key words

Chimeric *3D*-Gastruloids, mESCs, functional genetics, Tbx transcription factors, *Eomes*, *Brachyury*

Abstract

Stem cell-derived 3D-gastruloids show a remarkable capacity of self-organisation and recapitulate many aspects of gastrulation stage mammalian development. Gastruloids can be rapidly generated and offer several experimental advantages, such as scalability, observability, and accessibility for experimental manipulation. Here, we present innovative approaches to further expand the experimental potency of 3D-gastruloids by combining it with functional genetics in embryonic stem cells (ESCs) and the generation of chimeric gastruloids. Chimeric gastruloids are composed of fluorescently labelled cells of different genotypes for example cells with inducible gene-expression, or loss-of-gene function, combined with wildtype cells. We showcase the experimental approach and some advantages of chimeric gastruloids using ESCs carrying homozygous deletions of the Tbx transcription factors *Brachyury* or inducible expression of *Eomes.* The resulting chimeric gastruloids allowed to discriminate cell-autonomous from non-autonomous gene functions that normally are difficult to observe by genetics in the embryo.

Introduction

The versatile experimental opportunities offered by functional genetics available in the mouse as main mammalian model system have greatly enhanced our understanding of embryonic development. However, studies of mammalian embryogenesis are hampered by the relative inaccessibility of the embryo due to intrauterine growth. *Ex vivo* embryo cultures partially overcome some of the experimental restrictions but rely on the isolation of often limiting numbers of embryos. More recently, novel approaches were developed to generate stem cell derived, 3D-embryoids reflecting different stages of mammalian development from the formation of the blastocyst (Kagawa et al., 2022; Li et al., 2019; Yu et al., 2021), to periimplantation embryos (Amadei et al., 2021; Harrison et al., 2017; Harrison et al., 2018), and postimplantation stages recapitulating early organogenesis (Beccari et al., 2018; Moris et al., 2020; Turner et al., 2017; van den Brink et al., 2020; van den Brink et al., 2014; Veenvliet et al., 2020). These embryoid models demonstrate the remarkable self-organisation and robustness of embryonic programs that guide the processes of morphogenesis, growth, cell lineage specification and differentiation.

Among the most widely used embryoid model system are 3D-gastruloids, offering a simple experimental procedure to reproducibly generate embryoids that recapitulate development stages from early gastrulation to somitogenesis and onset of

organogenesis (comparable to Embryonic days 6.5 (E6.5) – E9.0) reviewed in (van den Brink and van Oudenaarden, 2021; Veenvliet et al., 2021). 3D-gastruloids are formed by the aggregation of 100-300 mouse or human pluripotent embryonic stem cells (ESCs) that are treated by a 24 h pulse of the GSK3β-inhibitor CHIR to activate the canonical Wnt-cascade. This signalling stimulus induces an anterior-posterior asymmetry in the aggregate (van den Brink et al., 2014), indicated by the one-sided expression of the Tbx factor *Brachyury* that in the embryo marks the site of primitive streak formation at gastrulation onset (Rivera-Perez and Magnuson, 2005; reviewed in Arnold and Robertson, 2009). The *Brachyury*-expressing posterior pole of 3D-gastruloids elongates over several days thereby forming different tissues resembling paraxial mesoderm, neural tube, and the primitive gut tube. 3D-gastruloids show a remarkable self-organizing capacity as the different tissues are generated in proper spatial organization and arranged according to the embryonic axes (Beccari et al., 2018). 3D-gastruloids thus can be used as model systems for studies of various gastrulation-associated morphogenetic processes, as exemplified for somitogenesis (van den Brink et al., 2020; Veenvliet et al., 2020). However, some tissues of gastrulation stage embryos are less represented in 3D-organoids, including anterior mesoderm derivatives, such as cardiogenic mesoderm, and cranial structures such as cranial neural tissues (van den Brink et al., 2020; Veenvliet et al., 2020). This underrepresentation of anterior/cranial tissues most likely results from the initial induction of ESC aggregates with CHIR which imposes a strong signal for posterior/caudal tissue identity (Dunty et al., 2008). However, this and other aberrations of 3D-gastruloids compared to embryos can also be used to investigate which additional regulatory requirements need to be met for proper morphogenesis of tissues and organ *anlagen* to more closely recapitulate the embryo (Veenvliet et al., 2021). Due to the scalability of this ESC- derived embryoid culture system, multiple different environmental cues can be readily tested. It is thus expected that further refinements of current protocols will lead to the generation of gastruloids that more closely resemble the different aspects of embryogenesis.

Cell specification to mesoderm and definitive endoderm (DE) cell lineages is regulated by two Tbx transcription factors *Eomesodermin* (*Eomes*) and *Brachyury (T)*. Functions of both factors were previously extensively studied establishing crucial roles of *Eomes* for cell lineage specification of definitive endoderm (DE) (Arnold et al., 2008; Teo et al., 2011) and anterior mesoderm (Costello et al., 2011), and functions of *Brachyury*

101 for the generation of posterior mesoderm derivatives, and notochord (Wymeersch et
102 al., 2021). The compound genetic deletion of *Eomes* and *Brachyury* completely
103 abrogates specification of any ME during differentiation of pluripotent cells (Tosic et
104 al., 2019). While functions of these Tbx factors for specification of cell fate are well
105 described, their roles in tissue-wide morphogenetic processes are less obvious. For
106 example, the genetic deletion of *Eomes* in the epiblast abrogates formation of the
107 mesoderm (and DE) cell layer, hindering studies of morphogenetic functions of *Eomes*-
108 regulated programs (Arnold et al., 2008). Similarly, studies of the role of *Brachyury* in
109 posterior body axis extension are compromised by cell non-autonomous functions of
110 *Brachyury* in feed-forward regulatory loops to maintain caudal Wnt-signals, also acting
111 on cell specification and morphogenetic programs (Arnold et al., 2000; Dunty et al.,
112 2008; Martin and Kimelman, 2008; Turner et al., 2014; Yamaguchi et al., 1999).
113 In this report, we demonstrate an approach to further expand the experimental potency
114 of 3D-gastruloids. We use genetically engineered, traceable ESCs to generate
115 chimeric 3D-gastruloids that are composed of cells with different genotypes. To
116 showcase the advantages of this approach and to test experimental feasibility we
117 generated fluorescently labelled ESC lines with homozygous loss-of-function, or
118 inducible expression cassettes for the two Tbx transcription factors *Eomes* and
119 *Brachyury*. These are used to generate chimeric gastruloids, e.g. by mixing inducible
120 Tbx-expressing, or Tbx-deficient and WT cells to generate complex genetic situations
121 that are normally only difficult to achieve by conventional genetic tools in embryos. In
122 addition to demonstrating the efficiency and feasibility of this experimental approach
123 of chimeric gastruloids, this study also provides insights into some of the
124 morphogenetic function of *Eomes* and *Brachyury*, which could not be achieved using
125 genetic approaches in embryos.
126

127 **Results and Discussion**

128 To expand the experimental versatility of the 3D-gastruloid model system we combined
129 it with the use of genetically modified ESCs and fluorescent imaging approaches. We
130 generated chimeric gastruloids composed of cells with different genetic backgrounds
131 that can be readily traced by microscopic observation using fluorescent membrane
132 labels (Fig. 1A, B). We generated WT ESCs that are permanently labelled by knock-in
133 of membrane GFP (mG) into the Rosa26 genomic locus (Fig. 1C). Membrane Tomato
134 (mT) labelling was used for genetically manipulated ESCs (Fig. 1C). Genetic

135 alterations used in presented experiments were the genetic deletion of the Tbx
136 transcription factor *Brachyury* (*Bra*$^{-/-}$), and the ICE-mediated (induced cassette
137 exchange) targeted integration of *Eomes* 3' to a Tet-responsive element (TRE) in A2lox
138 ESCs (Iacovino et al., 2014). We tested the generation of chimeric gastruloids by two
139 approaches (Fig. 1D, E). Either by mixing of different cells during the aggregation of
140 ESCs at the beginning of gastruloid culture (Fig. 1E), or by merging of two preformed
141 ESCs aggregates composed of different cells before CHIR-induction (Fig. 1D). ESC-
142 generated aggregates rapidly fuse and stably adhere after placing them together in 96-
143 wells (Fig. 1D) or in hanging drops (not shown). The mixing of cells at different ratios
144 can be used to evaluate cell-autonomous vs. cell non-autonomous gene functions, by
145 testing how different levels of cell contribution affects tissue-behaviour, e.g. when using
146 cells with loss-of-gene-function. Merging of cell aggregates can be applied when the
147 behaviour of coherent groups of cells is analysed, such as in studies of inductive tissue
148 interactions. A similar approach was recently reported where a small aggregate of 50
149 cells was treated with BMP4 to induce organizer-activities which was used instead of
150 CHIR-treatment for the induction of gastruloid-formation (Xu et al., 2021). Thus,
151 chimeric gastruloids offer multiple experimental opportunities to study gastrulation
152 development (Fig. 1A) as exemplarily demonstrated in following experiments.
153 First, we tested if chimeric gastruloids are a suitable model to study instructive gene
154 functions during lineage specification. Hence, we generated chimeric gastruloids by
155 merging preformed aggregates of WT ESCs (mG) and ESCs containing a doxycycline
156 (Dox) inducible GFP-tagged expression cassette for the Tbx factor *EomesGFP* (mT)
157 (Fig. 2A, B). *Eome*s is crucially required for lineage specification towards definitive
158 endoderm (Arnold et al., 2008; Teo et al., 2011) and anterior mesoderm, including the
159 cardiac lineage (Costello et al., 2011; Probst et al., 2021). We tested if forced *Eomes*
160 expression in a group of cells (TRE.*EomesGFP*) within a gastruloid would be sufficient
161 to induce a coherent heart-like domain, which is only inconsistently occurring in
162 gastruloids formed of WT ESCs (Rossi et al., 2021; van den Brink and van
163 Oudenaarden, 2021). Indeed, Dox-induced *EomesGFP*-expressing cells form a
164 domain of beating cardiomyocytes (Fig. 2C, Supplementary movie 2) in chimeric
165 gastruloids in more than 30% of cases, whereas similar beating areas are only very
166 rarely observed in uninduced chimeric gastruloids (Fig. 2D) or using only A2lox WT
167 ESCs (not shown). To correlate induced *EomesGFP* expression with the cardiogenic
168 domain we performed *in situ* hybridization analyses for early cardiac markers *Mlc2a*

169 and *Nkx2.5*, which are found almost exclusively in mT-marked TRE.*EomesGFP* cells
170 that are forming a coherent domain on one side of gastruloids (Fig. 2E). This
171 experiment thus shows that induced expression of *Eomes* suffices to cell-
172 autonomously generate coherent cardiogenic domains oriented to one side of the
173 developing gastruloid, resembling the embryonic localization of heart formation.
174 Next, we aimed for testing the feasibility of chimeric gastruloids for the assessment of
175 cell-autonomous vs. cell non-autonomous functions of *Brachyury* during posterior
176 elongation, as the shortening of the posterior body axis is the most prominent
177 phenotype of *Brachyury*-mutant embryos (Fig. 3A)(Wymeersch et al., 2021).
178 Gastruloids entirely generated from mT-labelled *Bra*$^{-/-}$ mESCs present with a
179 phenotype of impaired elongation, similar to shortened tailbuds observed in *Brachyury*-
180 mutant embryos (Fig. 3B, C) (Inman and Downs, 2006). Increasing the proportional
181 contribution of WT cells (mG) to the gastruloid by intermixing WT with *Bra*$^{-/-}$ mESCs
182 during the initial aggregation of 300 ESCs leads to the gradual extension and increase
183 in overall mass of the posterior portion of the mixed gastruloids (Fig. 3C). Interestingly,
184 in the tail bud region of chimeric gastruloids with a contribution of *Bra*$^{-/-}$ cells of 90%,
185 *Brachyury* expression is also absent in WT cells when compared to chimeric
186 gastruloids where *Bra*$^{-/-}$ cell contribution is only 50%, and Brachyury expression is
187 robustly induced in the posterior pole (Fig. 3D). The cell non-autonomous contribution
188 of *Bra*$^{-/-}$ cells to disturbances of axis-extension is most likely explained by the previously
189 described feed-forward regulation of *Wnt3a* and *Brachyury* in the tail-bud region
190 (Arnold et al., 2000; Dunty et al., 2008; Martin and Kimelman, 2008; Turner et al., 2014;
191 Yamaguchi et al., 1999).
192 Finally, in addition to the gross, tissue-wide phenotype of *Brachyury*-deficiency in
193 gastruloids with a high ratio of *Bra*$^{-/-}$ cells, we analyzed the cell-autonomous effects of
194 *Brachyury*-deficiency in conditions of low contribution of mutant cells (Fig. 4). We
195 generated chimeric gastruloids by mixing cells in a 90:10 ration of WT and *Bra*$^{-/-}$ ESCs,
196 respectively. In resulting gastruloids *Bra*$^{-/-}$ cells show a specific tissue distribution, so
197 that they are predominantly found along the midline in the interior of the gastruloids,
198 and in the posterior pole (Fig. 4A). To determine tissue identity of these regions we
199 used immunofluorescence (IF) staining against FOXA2 and CDH1 (E-Cadherin),
200 labelling DE (Viotti et al., 2014) and SOX2, labelling neuroectoderm (NE) cells (Wood
201 and Episkopou, 1999), and combined IF-staining with the fluorescent labels of WT
202 (mG) and *Bra*$^{-/-}$ cells (mT) (Fig. 4B, C). FOXA2 and CDH1 stainings indicate that *Bra*$^{-/-}$

203 cells are biased towards DE and are favored to form the gut tube-like structure in the
204 midline. This finding demonstrates not only that *Brachyury* is dispensable for DE
205 lineage specification from pluripotent cells, but suggests that *Brachyury* actually
206 counteracts DE specification programs and thus may not represent a suitable marker
207 for early DE-forming cells as previously suggested (Kubo et al., 2004). Staining against
208 SOX2 shows that the *Bra*$^{-/-}$ cells that are present in the posterior pole of chimeric
209 gastruloids mostly acquire NE fate, in accordance with previous findings about NE-
210 repressive functions of *Brachyury* (Koch et al., 2017; Tosic et al., 2019).
211 In conclusion, this study illustrates a novel experimental approach by combining
212 functional genetics in ESCs with 3D-gastruloids to form different types of chimeric
213 gastruloids, that allow to experimentally address various aspects of development.
214 Inducible expression of the Tbx transcription factor *Eomes* demonstrates how
215 limitations of 3D gastruloids can be overcome by genetically providing regulatory cues
216 that are missing or underrepresented in CHIR-only treated gastruloids, namely the
217 induced formation of anterior mesoderm derivatives such as heart tissue. We
218 additionally show how chimeric gastruloids can be employed to analyze cell-
219 autonomous and cell non-autonomous gene-functions by varying the contribution of
220 gene-mutant cells to chimeric gastruloids. Using a low ratio of only 10% of *Brachyury*-
221 deficient cells we find that *Bra*$^{-/-}$ cells cell-autonomously are biased towards the DE, a
222 cell lineage that strictly depends on *Eomes* functions (Arnold et al., 2008; Teo et al.,
223 2011). Since *Brachyury* and *Eomes* are co-expressed in cells of the early primitive
224 streak in early gastrulating embryos (Probst et al., 2021), this poses the interesting
225 question about the regulatory interactions between these two related Tbx factors.
226 While in this study we used functional genetics of ESCs harbouring loss- and gain-of-
227 gene function alleles, ESCs with other genetic modifications could also be applied in
228 chimeric gastruloids, for example reporter-containing cells for signalling pathway (e.g.
229 Wnt-signalling), cellular processes (e.g. cell migration and actin-dynamics), or protein-
230 localization. Additionally, while in this study chimeric gastruloids contained only two
231 different cell types, more cells of different genotype could be combined. This might be
232 desirable, e.g. to observe morphogenetic processes by different reporter cell lines.
233 In summary, chimeric gastruloids represent powerful experimental tools for studies of
234 gastrulation stage embryogenesis. In addition to the increased experimental
235 accessibility, observability and scalability, chimeric gastruloids also allow to generate

236 complex genetic settings that are normally only difficult to achieve by genetics in
237 embryos.
238
239 **Materials and Methods**
240 **Cell lines**
241 A2lox mouse ESCs (Iacovino et al., 2014) were cultured in Dulbecco's modified
242 Eagle's medium (DMEM) containing 15 % fetal bovine serum (FBS, Gibco), 2 mM L-
243 glutamine, 1X non-essential amino acids (NEAA), 1 mM sodium-pyruvate, 1X
244 penicillin/streptomycin (all from Gibco), 100 µM β-mercaptoethanol (Sigma), Leukemia
245 inhibitory factor (ESGRO LIF, Merck Millipore, 1000 U/ml), and 2i: CHIR99021 (Axon
246 Medchem, 3 µM) and PD0325901 (Axon Medchem, 1 µM) on 0.1% gelatine-coated
247 dishes. The medium was changed daily and ESCs were passaged every other day.
248 The generation of *Bra*$^{-/-}$ ESCs and of A2lox ESCs harbouring dox- inducible expression
249 cassette for *Eomes*.GFP were described previously (Tosic et al., 2019). A2lox cells
250 with membrane-tagged fluorescent labels (membrane-Tomato, mT, and membrane-
251 GFP, mG) were generated by targeted integration of a mT/mG targeting vector
252 (Muzumdar et al., 2007), Addgene plasmid #17787) into the Rosa26 locus. 1x10^{6} A2lox
253 ESCs (WT and *Bra*$^{-/-}$) were transfected with 2.5 µg of linearized vector using the
254 Nucleofector ESC kit (Lonza) and G418 selected (350 µg/ml) on a monolayer of MitoC
255 (Sigma)-mitotically inactivated STO feeder cells. mT-expressing ESC clones were
256 picked on day 9 of selection. To convert the expression of the membrane-Tomato (mT)
257 to membrane-GFP (mG) in WT A2lox ESCs, cells were treated for 24 h with 5 µg/ml
258 Doxycyclin (Sigma, D9891) for induced expression of the Cre-recombinase from the
259 Dox-inducible locus of A2lox WT cells to excise the loxP-flanked mT expression
260 cassette and bring the mG expression cassette under the transcriptional control of the
261 Rosa26 gene locus. After Cre-excision mG-expressing WT A2lox ESCs underwent one
262 round of clonal selection by minimal dilution of 500 cells onto a 10 cm cell culture dish.
263
264 **Generation of chimeric gastruloids**
265 Gastruloids were generated using published protocols (van den Brink et al., 2020) with
266 some modifications as outlined below. Gastruloid formation was performed in ESGRO
267 Complete Basal Medium (Merck Millipore) in the absence of Matrigel. To generate
268 chimeric gastruloids using different ESCs by merging of preformed aggregates 150
269 cells of each ESC line were aggregated in 40 µl of ESGRO basal medium in 96-well

270 format (Greiner ultra-low attachment plates, No. 650970) for 24 h before merging by
271 combining two aggregates into the same well. At 48 h following first aggregate
272 formation, fused gastruloids were induced by administration of 3 µM CHIR and if
273 indicated with doxycycline (1 µg/µl, Sigma) for 24 h. In the course of gastruloid culture,
274 the medium was changed daily at 72, 96, 120 and 144 h. For the generation of
275 gastruloids by mixing of different ESC lines, aggregates were formed from a total of
276 300 ESCs at various rations between the two ESC lines, and further gastruloid
277 formation followed by previously used protocols (van den Brink et al., 2020).
278
279 **Whole mount *in situ* hybridization**
280 Whole-mount in situ hybridization was performed according to standard protocols
281 using previously published probes for *Mlc2a* and *Nkx2.5* (Costello et al., 2011). In brief,
282 gastruloids were fixed in 4% PFA / PBS o/n at 4°C, dehydrated and stored in methanol
283 at -20°C. After rehydration gastrulation were bleached in 6 % H_2O_2 for 5 min, digested
284 by 1.6 µg / ml Proteinase K in PBT for 2 min, and postfixed in 4% PFA / 0,2%
285 glutaraldehyde for 20 min before prehybridization for 2 h and hybridization o/n
286 according to standard protocols. DIG-labelled RNA probe was detected using anti-
287 Digoxigenin-AP Fab fragments (Roche) in 1% sheep serum, 2% BBR in MAB (0.1 M
288 Maleic acid, 0.3 M NaCl, NaOH, 1% Tween-20 in H_2O, pH 7.5) and incubation at 4°C
289 o/n. Antibody was washed out by extensive washes in MAB (>24 h, RT), and color
290 reaction performed in BM purple staining solution (Roche) for 2-6 h at RT.
291
292 **Immunofluorescence staining**
293 Gastruloids were fixed in 4% PFA /PBS for 1 h at 4°C, permeabilized (0.3% Triton X-
294 100/ PBT, 30 min) and blocked in 1% BSA / PBT for 1h at RT. Primary antibody
295 incubation was performed at 4°C o/n in 1% BSA / PBT, gastruloids washed 4x in PBT
296 before secondary fluorescence-conjugated antibody incubation for 3 h followed by
297 DAPI staining for 30 min at RT. Primary antibodies used were BRACHYURY (R&D
298 Systems; AF2085), FOXA2 (Cell Signaling; 8186S), E-Cadherin (BD Transduction
299 Laboratories; 610182) and SOX2 (R&D Systems; AF2018) at suggested dilutions.
300 Secondary anti-goat, anti-rabbit and anti-mouse Alexa Fluor 647-conjugated
301 antibodies (Thermo Fisher) were used at 1:1000 dilutions.
302
303 **Imaging**

Images were acquired on a Leica DMi8 Thunder Imager System or a Leica M165FC Stereo microscope. Images were processed in the Leica LASX software and Affinity Photo. During time lapse imaging gastruloids were maintained under constant conditions at 37°C, 5% CO_2.

Acknowledgements

We thank T. Bass for excellent technical assistance and Michael Kyba for the A2lox ESC line.

Funding

This work was supported by the German Research Foundation (DFG) through the Heisenberg Program (AR 732/3-1), project grant (AR 732/2-1,) project B07 of SFB 1140 (project ID 246781735), project A03 of SFB 850 (project ID 89986987), project P7 of SFB 1453 (project ID 431984000), and Germany's Excellence Strategy (CIBSS – EXC-2189 – Project ID 390939984) to S.J.A., and by the MOTI-VATE program of the Freiburg Medical Faculty supported by the Else-Kröner-Fresenius-Stiftung to A.C.

Competing interests

The authors declare no competing interests.

Author contributions

A.E.W., K.M.S., A.C., C.M.S. generated different ESC lines and performed experiments. A.E.W, S.P. and S.J.A. planned and analyzed experiments. A.E.W. and S.J.A. prepared figures, wrote and edited the manuscript with input from all authors. S.J.A. conceived the study.

References

Amadei, G., Lau, K. Y. C., De Jonghe, J., Gantner, C. W., Sozen, B., Chan, C., Zhu, M., Kyprianou, C., Hollfelder, F. and Zernicka-Goetz, M. (2021). Inducible Stem-Cell-Derived Embryos Capture Mouse Morphogenetic Events In Vitro. *Dev Cell* **56**, 366-382 e369.

Arnold, S. J., Hofmann, U. K., Bikoff, E. K. and Robertson, E. J. (2008). Pivotal roles for eomesodermin during axis formation, epithelium-to-mesenchyme transition and endoderm specification in the mouse. *Development* **135**, 501-511.

338 **Arnold, S. J. and Robertson, E. J.** (2009). Making a commitment: cell lineage allocation and
339 axis patterning in the early mouse embryo. *Nat Rev Mol Cell Biol* **10**, 91-103.
340 **Arnold, S. J., Stappert, J., Bauer, A., Kispert, A., Herrmann, B. G. and Kemler, R.** (2000).
341 Brachyury is a target gene of the Wnt/beta-catenin signaling pathway. *Mech Dev* **91**, 249-
342 258.
343 **Beccari, L., Moris, N., Girgin, M., Turner, D. A., Baillie-Johnson, P., Cossy, A. C., Lutolf,**
344 **M. P., Duboule, D. and Arias, A. M.** (2018). Multi-axial self-organization properties of
345 mouse embryonic stem cells into gastruloids. *Nature* **562**, 272-276.
346 **Costello, I., Pimeisl, I. M., Drager, S., Bikoff, E. K., Robertson, E. J. and Arnold, S. J.**
347 (2011). The T-box transcription factor Eomesodermin acts upstream of Mesp1 to specify
348 cardiac mesoderm during mouse gastrulation. *Nat Cell Biol* **13**, 1084-1091.
349 **Dunty, W. C., Jr., Biris, K. K., Chalamalasetty, R. B., Taketo, M. M., Lewandoski, M. and**
350 **Yamaguchi, T. P.** (2008). Wnt3a/beta-catenin signaling controls posterior body
351 development by coordinating mesoderm formation and segmentation. *Development* **135**,
352 85-94.
353 **Harrison, S. E., Sozen, B., Christodoulou, N., Kyprianou, C. and Zernicka-Goetz, M.**
354 (2017). Assembly of embryonic and extraembryonic stem cells to mimic embryogenesis
355 in vitro. *Science* **356**.
356 **Harrison, S. E., Sozen, B. and Zernicka-Goetz, M.** (2018). In vitro generation of mouse
357 polarized embryo-like structures from embryonic and trophoblast stem cells. *Nat Protoc*
358 **13**, 1586-1602.
359 **Iacovino, M., Roth, M. E. and Kyba, M.** (2014). Rapid genetic modification of mouse
360 embryonic stem cells by Inducible Cassette Exchange recombination. *Methods Mol Biol*
361 **1101**, 339-351.
362 **Inman, K. E. and Downs, K. M.** (2006). Brachyury is required for elongation and
363 vasculogenesis in the murine allantois. *Development* **133**, 2947-2959.
364 **Kagawa, H., Javali, A., Khoei, H. H., Sommer, T. M., Sestini, G., Novatchkova, M., Scholte**
365 **Op Reimer, Y., Castel, G., Bruneau, A., Maenhoudt, N., et al.** (2022). Human blastoids
366 model blastocyst development and implantation. *Nature* **601**, 600-605.
367 **Koch, F., Scholze, M., Wittler, L., Schifferl, D., Sudheer, S., Grote, P., Timmermann, B.,**
368 **Macura, K. and Herrmann, B. G.** (2017). Antagonistic Activities of Sox2 and Brachyury
369 Control the Fate Choice of Neuro-Mesodermal Progenitors. *Dev Cell* **42**, 514-526 e517.
370 **Kubo, A., Shinozaki, K., Shannon, J. M., Kouskoff, V., Kennedy, M., Woo, S., Fehling, H.**
371 **J. and Keller, G.** (2004). Development of definitive endoderm from embryonic stem cells
372 in culture. *Development* **131**, 1651-1662.

373 **Li, R., Zhong, C., Yu, Y., Liu, H., Sakurai, M., Yu, L., Min, Z., Shi, L., Wei, Y., Takahashi,**
374 **Y., et al.** (2019). Generation of Blastocyst-like Structures from Mouse Embryonic and
375 Adult Cell Cultures. *Cell* **179**, 687-702 e618.
376 **Martin, B. L. and Kimelman, D.** (2008). Regulation of canonical Wnt signaling by Brachyury
377 is essential for posterior mesoderm formation. *Dev Cell* **15**, 121-133.
378 **Moris, N., Anlas, K., van den Brink, S. C., Alemany, A., Schroder, J., Ghimire, S., Balayo,**
379 **T., van Oudenaarden, A. and Martinez Arias, A.** (2020). An in vitro model of early
380 anteroposterior organization during human development. *Nature* **582**, 410-415.
381 **Muzumdar, M. D., Tasic, B., Miyamichi, K., Li, L. and Luo, L.** (2007). A global double-
382 fluorescent Cre reporter mouse. *Genesis* **45**, 593-605.
383 **Probst, S., Sagar, Tosic, J., Schwan, C., Grun, D. and Arnold, S. J.** (2021). Spatiotemporal
384 sequence of mesoderm and endoderm lineage segregation during mouse gastrulation.
385 *Development* **148**.
386 **Rivera-Perez, J. A. and Magnuson, T.** (2005). Primitive streak formation in mice is preceded
387 by localized activation of Brachyury and Wnt3. *Dev Biol* **288**, 363-371.
388 **Rossi, G., Broguiere, N., Miyamoto, M., Boni, A., Guiet, R., Girgin, M., Kelly, R. G., Kwon,**
389 **C. and Lutolf, M. P.** (2021). Capturing Cardiogenesis in Gastruloids. *Cell Stem Cell* **28**,
390 230-240 e236.
391 **Teo, A. K., Arnold, S. J., Trotter, M. W., Brown, S., Ang, L. T., Chng, Z., Robertson, E. J.,**
392 **Dunn, N. R. and Vallier, L.** (2011). Pluripotency factors regulate definitive endoderm
393 specification through eomesodermin. *Genes Dev* **25**, 238-250.
394 **Tosic, J., Kim, G. J., Pavlovic, M., Schroder, C. M., Mersiowsky, S. L., Barg, M., Hofherr,**
395 **A., Probst, S., Kottgen, M., Hein, L., et al.** (2019). Eomes and Brachyury control
396 pluripotency exit and germ-layer segregation by changing the chromatin state. *Nat Cell*
397 *Biol* **21**, 1518-1531.
398 **Turner, D. A., Girgin, M., Alonso-Crisostomo, L., Trivedi, V., Baillie-Johnson, P.,**
399 **Glodowski, C. R., Hayward, P. C., Collignon, J., Gustavsen, C., Serup, P., et al.**
400 (2017). Anteroposterior polarity and elongation in the absence of extra-embryonic tissues
401 and of spatially localised signalling in gastruloids: mammalian embryonic organoids.
402 *Development* **144**, 3894-3906.
403 **Turner, D. A., Rue, P., Mackenzie, J. P., Davies, E. and Martinez Arias, A.** (2014).
404 Brachyury cooperates with Wnt/beta-catenin signalling to elicit primitive-streak-like
405 behaviour in differentiating mouse embryonic stem cells. *BMC Biol* **12**, 63.
406 **van den Brink, S. C., Alemany, A., van Batenburg, V., Moris, N., Blotenburg, M., Vivie, J.,**
407 **Baillie-Johnson, P., Nichols, J., Sonnen, K. F., Martinez Arias, A., et al.** (2020). Single-
408 cell and spatial transcriptomics reveal somitogenesis in gastruloids. *Nature* **582**, 405-409.

409 **van den Brink, S. C., Baillie-Johnson, P., Balayo, T., Hadjantonakis, A. K., Nowotschin,**
410 **S., Turner, D. A. and Martinez Arias, A.** (2014). Symmetry breaking, germ layer
411 specification and axial organisation in aggregates of mouse embryonic stem cells.
412 *Development* **141**, 4231-4242.
413 **van den Brink, S. C. and van Oudenaarden, A.** (2021). 3D gastruloids: a novel frontier in
414 stem cell-based in vitro modeling of mammalian gastrulation. *Trends Cell Biol* **31**, 747-
415 759.
416 **Veenvliet, J. V., Bolondi, A., Kretzmer, H., Haut, L., Scholze-Wittler, M., Schifferl, D.,**
417 **Koch, F., Guignard, L., Kumar, A. S., Pustet, M., et al.** (2020). Mouse embryonic stem
418 cells self-organize into trunk-like structures with neural tube and somites. *Science* **370**.
419 **Veenvliet, J. V., Lenne, P. F., Turner, D. A., Nachman, I. and Trivedi, V.** (2021). Sculpting
420 with stem cells: how models of embryo development take shape. *Development* **148**.
421 **Viotti, M., Nowotschin, S. and Hadjantonakis, A. K.** (2014). SOX17 links gut endoderm
422 morphogenesis and germ layer segregation. *Nat Cell Biol* **16**, 1146-1156.
423 **Wood, H. B. and Episkopou, V.** (1999). Comparative expression of the mouse Sox1, Sox2
424 and Sox3 genes from pre-gastrulation to early somite stages. *Mech Dev* **86**, 197-201.
425 **Wymeersch, F. J., Wilson, V. and Tsakiridis, A.** (2021). Understanding axial progenitor
426 biology in vivo and in vitro. *Development* **148**.
427 **Xu, P. F., Borges, R. M., Fillatre, J., de Oliveira-Melo, M., Cheng, T., Thisse, B. and Thisse,**
428 **C.** (2021). Construction of a mammalian embryo model from stem cells organized by a
429 morphogen signalling centre. *Nat Commun* **12**, 3277.
430 **Yamaguchi, T. P., Takada, S., Yoshikawa, Y., Wu, N. and McMahon, A. P.** (1999). T
431 (Brachyury) is a direct target of Wnt3a during paraxial mesoderm specification. *Genes*
432 *Dev* **13**, 3185-3190.
433 **Yu, L., Wei, Y., Duan, J., Schmitz, D. A., Sakurai, M., Wang, L., Wang, K., Zhao, S., Hon,**
434 **G. C. and Wu, J.** (2021). Blastocyst-like structures generated from human pluripotent
435 stem cells. *Nature* **591**, 620-626.

436

437 **FIGURE LEGENDS**

438 **Fig. 1. Experimental approaches for the generation of chimeric gastruloids**

439 **(A)** Schematic of two alternative experimental approaches to generate chimeric
440 gastruloids from fluorescently labelled embryonic stem cells (ESCs). Wildtype (WT)
441 ESCs are marked by membrane-GFP (mG) and combined with membrane-Tomato
442 (mT) labelled, genetically modified ESCs. The genetic modifications of ESCs comprise
443 homozygous gene deletions (GeneX) or inducible gene-expression by the targeting of
444 cDNAs into a fully controllable pre-engineered locus containing a Tetracycline

445 responsive element (TRE) for dox-dependent induction of gene expression (GeneY).
446 Chimeric gastruloids are generated by either mixing of ESCs at the beginning of
447 gastruloid culture, or by merging preformed ESCs aggregates proceeding the induction
448 of gastruloids by CHIR. Chimeric gastruloids can be used as versatile novel model
449 system for various types of studies and embryonic research questions as indicated
450 exemplary.
451 **(B)** Schematic of the protocol to form chimeric gastruloids indicating timepoints for
452 either mixing of cells, or merging of aggregates to create chimeric gastruloids.
453 **(C)** Membrane-GFP (mG) labelling of WT ESCs and membrane-Tomato (mT) labelling
454 for genetically modified ESCs allows for distinguishing different cell types in chimeric
455 gastruloids. Scale bars 10 µm.
456 **(D)** Timelapse-imaging of the merging process of pre-formed ESC aggregates at
457 indicated time points. 150 mG and mT ESCs were aggregated for 24 h before merging
458 them by placing them together in 96-well plates. After 1 hr two aggregates
459 spontaneously aggregated and formed stable contacts. Scale bars 100 µm. Also see
460 **Supplementary Movie 1** for a 12 h time-lapse movie.
461 **(E)** Examples of mixed ESC aggregates at 24 h after aggregation of 300 ESCs by
462 mixing mG WT ESCs and mT Bra$^{-/-}$ ESCs at indicated rations. Scale bars 100µm.
463
464 **Fig. 2. Instructive functions of *Eomes* for cardiac lineage specification in merged**
465 **chimeric gastruloids.**
466 **(A)** Schematic illustrating the generation and culture of chimeric gastruloids by merging
467 preformed aggregated of mG-labelled WT ESCs and mT-labelled ESCs harbouring
468 *EomesGFP* in the Doxycycline (Dox)-inducible gene locus (TRE.*EomesGFP, short*
469 TRE.*Eo*).
470 **(B)** Fluorescent microscopy of TRE.*EomesGFP* ESCs showing nuclear staining of
471 doxycycline-induced (+DOX) EOMES.GFP after 24 h of administration that is absent
472 in -DOX conditions. Scale bars 10 µm.
473 **(C)** Brightfield (left) and fluorescent (right) images of a chimeric gastruloid following
474 induced *Eomes* expression showing the region of beating cardiomyocytes within the
475 gastruloid that is mostly derived of mT-labelled TRE.*EomesGFP* cells. The dashed line
476 indicates the domain of beating cells. Scale bars 100 µm. See also **Supplementary**
477 **Movie 2** for the corresponding time-lapse movie.

478 **(D)** Statistics comparing the percentage of beating gastruloids at 168 h following forced
479 *Eomes* expression +DOX (33,3% ± 3,01) and uninduced controls -DOX (1,5% ± 2,31)
480 in n=3 independent experiments. Error bar indicates SEM.
481 **(E)** Fluorescent microscopy (left) and whole-mount *in situ* hybridization (right) of the
482 same chimeric gastruloids following induced *Eomes*-expression (+DOX) shows the
483 instructive functions of forced *Eomes*-expression in TRE.*EomesGFP* cells for the
484 induction of cardiac progenitors, indicated by expression of *Mlc2a* and *Nkx2.5.* Scale
485 bars 100 µm.
486
487 **Fig. 3. Analyses of *Brachyury* functions during axis-elongation in chimeric**
488 **gastruloids generated by cell mixing.**
489 **(A)** Schematic illustrating the generation of chimeric gastruloids by mixing of mG-
490 labelled WT ESCs and mT-labelled Brachyury-deficient (*Bra*$^{-/-}$) ESCs.
491 **(B)** Immunofluorescence stainings for BRACHYURY in gastruloids at 120 h generated
492 from either WT or *Bra*$^{-/-}$ cells showing the presence of BRACHYURY in the posterior
493 pole of the WT, and absence in *Bra*$^{-/-}$ derived gastruloids that fail to elongate.
494 **(C)** Chimeric gastruloids at 120 h generated by mixing of *Bra*$^{-/-}$ (mT) and WT (mG)
495 ESCs at indicated rations of cell numbers. Gastruloids with a contribution of *Bra*$^{-/-}$ cells
496 above 80 % show reduced axial elongation. Gastruloids entirely generated from *Bra*$^{-/-}$
497 cells fail to extend beyond an oval shape. At WT (mG) cell contribution > 50 % axial
498 elongation is similar to WT gastruloids but occasionally shows a thinning of the
499 posterior portion. Across all experiments *Bra*$^{-/-}$ (mT) cells preferentially contribute to the
500 posterior portion of mixed gastruloids. In all images anterior is to the top and posterior
501 to the bottom of the picture.
502 **(D)** Immunofluorescence staining for BRACHYUY in gastruloids generated by cell
503 mixing of *Bra*$^{-/-}$ and WT in rations of 90:10 and 50:50 show the absence of BRACHYUY
504 from WT cells (arrows) at the posterior pole in gastruloids with a high contribution of
505 *Bra*$^{-/-}$ cells (90% contribution) by cell non-autonomous mechanisms. Scale bars 100
506 µm in B-D.
507
508 **Fig. 4. Cell-autonomous effects of Brachyury-deficiency on cell lineage**
509 **specification and tissue sorting in chimeric gastruloids with low contribution of**
510 ***Bra*$^{-/-}$ cells**

511 **(A)** Three independent replicates of chimeric gastruloids at 120 h generated by mixing
512 of 10% *Bra*$^{-/-}$ (mT) and 90 % WT (mG) ESCs at the start of the experiment show an
513 enrichment of *Bra*$^{-/-}$ cells along the midline of the gastruloids and the posterior pole.
514 The three replicates indicate the spectrum of distribution of *Bra*$^{-/-}$ cells found in chimeric
515 gastruloids.
516 **(B)** Immunofluorescence stainings for the definitive endoderm marker FOXA2 and the
517 epithelial marker CDH1 (E-Cadherin) show the predominant contribution of *Bra*$^{-/-}$ cells
518 to endoderm-like cells forming the primary gut tube (arrow) of gastruloids, and some
519 enrichment of *Bra*$^{-/-}$ cells in the posterior region, reflecting the tail bud region (boxed).
520 **(C)** *Bra*$^{-/-}$ cells that don't contribute to the epithelial primary gut tube of mixed
521 gastruloids show nuclear SOX2-staining suggesting lineage commitment to
522 neuroectoderm cell types. Scale bars 100 µm in A-C.
523

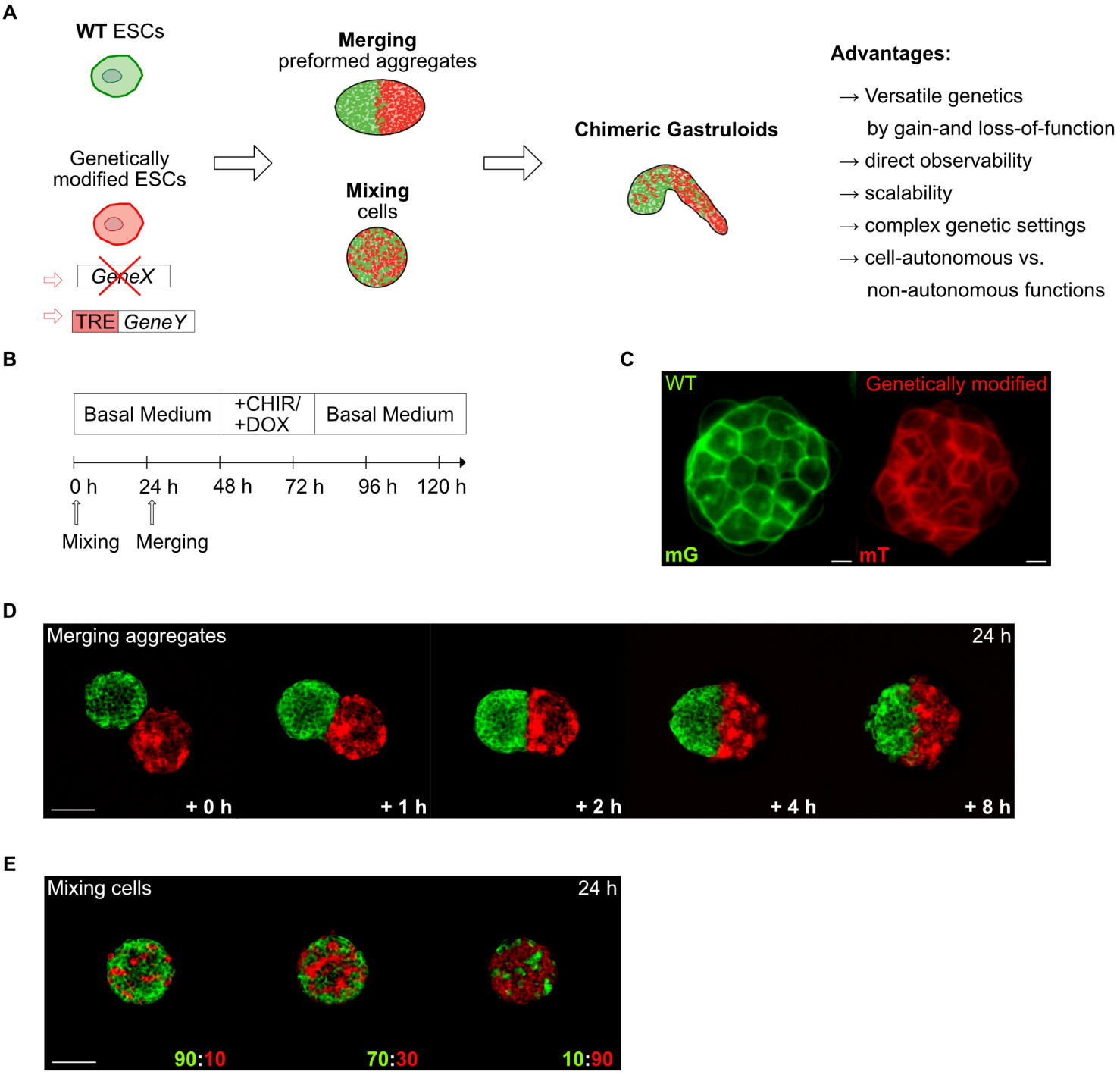
A
WT ESCs
Genetically modified ESCs
GeneX
TRE GeneY
Merging
preformed aggregates
Mixing
cells
Chimeric Gastruloids
Advantages:
→ Versatile genetics by gain-and loss-of-function
→ direct observability
→ scalability
→ complex genetic settings
→ cell-autonomous vs. non-autonomous functions
B
Basal Medium
+CHIR/ +DOX
Basal Medium
0 h
24 h
48 h
72 h
96 h
120 h
Mixing
Merging
C
WT
Genetically modified
mG
mT
D
Merging aggregates
24 h
+ 0 h
+ 1 h
+ 2 h
+ 4 h
+ 8 h
E
Mixing cells
24 h
90:10
70:30
10:90

Fig. 1

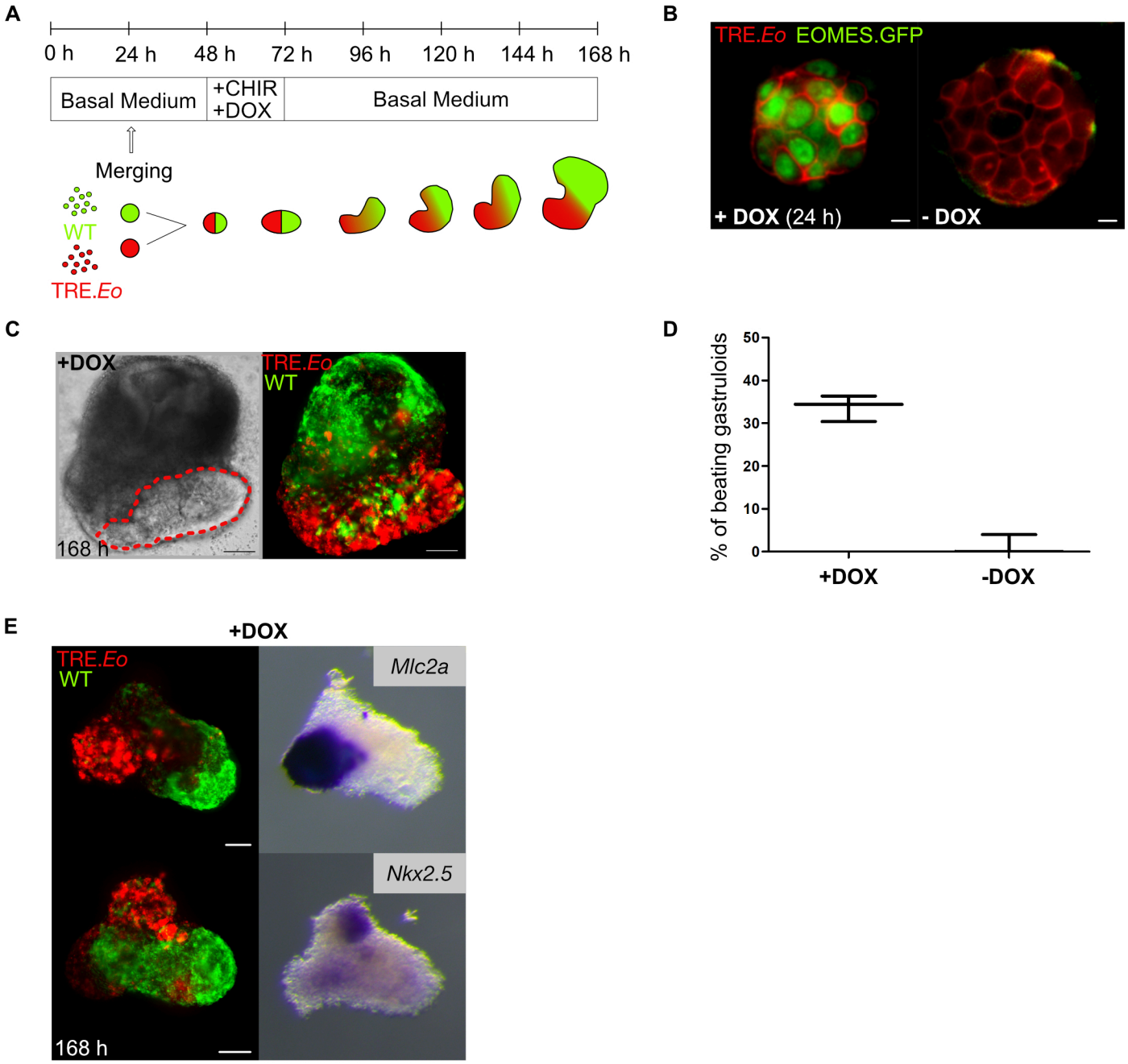
A
0 h
24 h
48 h
72 h
96 h
120 h
144 h
168 h
Basal Medium
+CHIR
+DOX
Basal Medium
Merging
WT
TRE.Eo
B
TRE.Eo EOMES.GFP
+ DOX (24 h)
- DOX
C
+DOX
TRE.Eo
WT
168 h
D
% of beating gastruloids
50
40
30
20
10
0
+DOX
-DOX
E
+DOX
TRE.Eo
WT
Mlc2a
Nkx2.5
168 h

Fig. 2

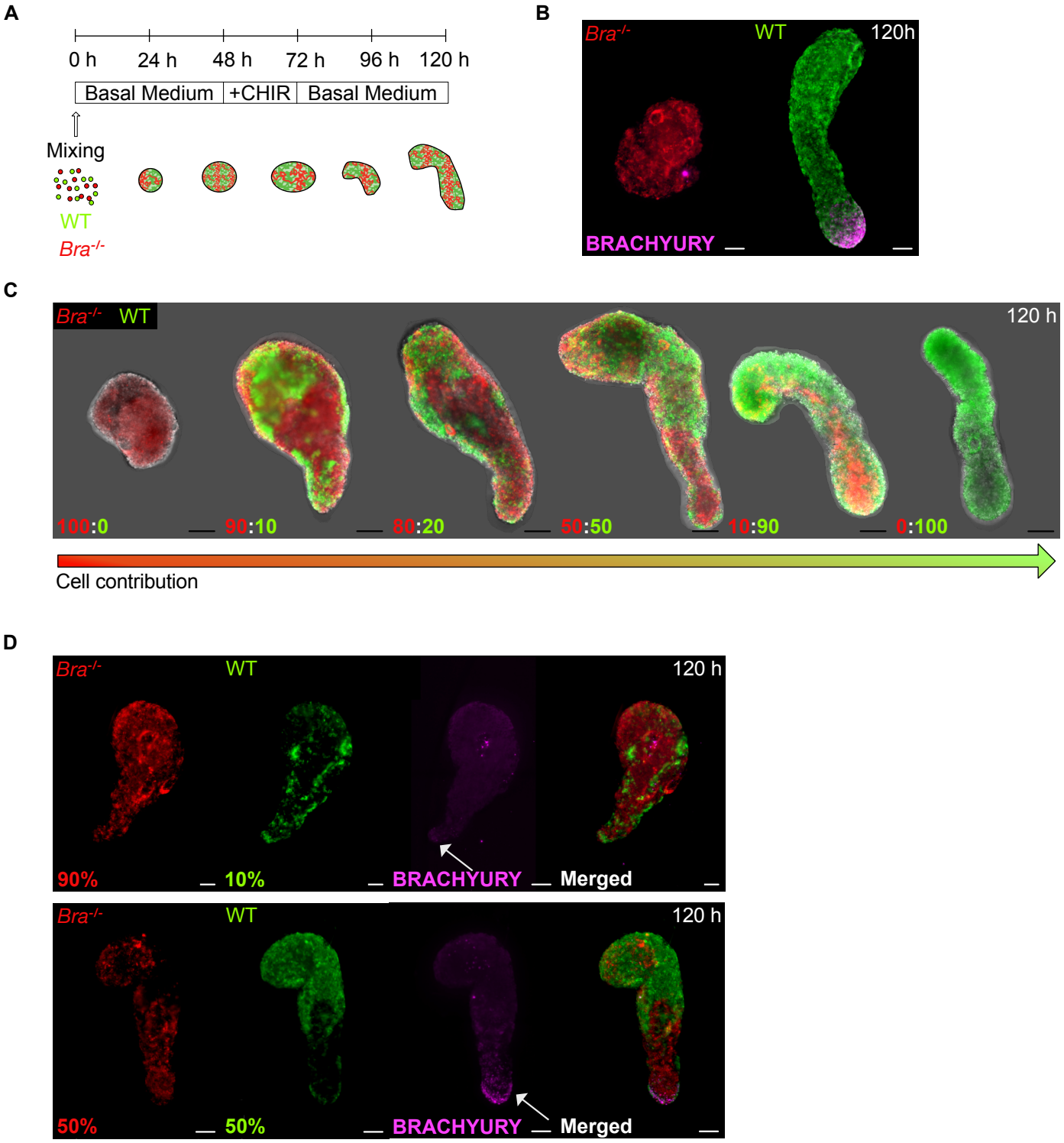
A
0 h
24 h
48 h
72 h
96 h
120 h
Basal Medium
+CHIR
Basal Medium
Mixing
WT
Bra-/-
B
Bra-/-
WT
120h
BRACHYURY
C
Bra-/-
WT
120 h
100:0
90:10
80:20
50:50
10:90
0:100
Cell contribution
D
Bra-/-
WT
120 h
90%
10%
BRACHYURY
Merged
Bra-/-
WT
120 h
50%
50%
BRACHYURY
Merged

Fig. 3

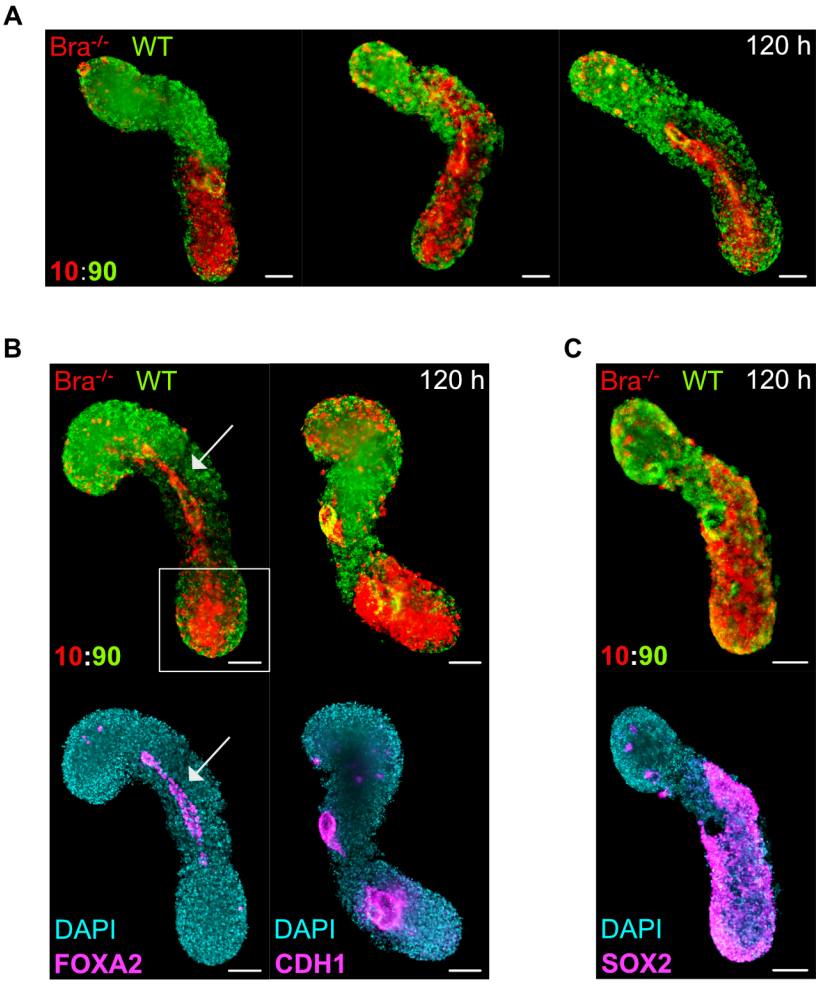
A
Bra-/- WT
120 h
10:90
B
Bra-/- WT
120 h
10:90
DAPI
FOXA2
DAPI
CDH1
C
Bra-/- WT
120 h
10:90
DAPI
SOX2

Fig. 4